External Magnetic Field-Induced Targeted Delivery of Highly Sensitive Iron Oxide Nanocubes for MRI of Myocardial Infarction

Bingbing Hu, Mu Zeng, Jingli Chen, Zhenzhong Zhang, Xiaoning Zhang, Zhanming Fan, and Xin Zhang**

Myocardial infarction (MI) and associated sequelae continue to be a major cause of morbidity and mortality in developed and developing countries.[1] MI occurs through the processes of cellular necrosis and apoptosis initiated by ischemia and reperfusion.[2a,b] During MI, the loss of coronary blood flow leads to the processes of cellular necrosis and apoptosis, which can activate the complement and cytokine cascades and make monocytes differentiate into macrophages in the infarcted tissue.[2c,d] Then neutrophils and macrophages serve to clear away dead cells and other necrotic debris.[2e] Given the complex process, the methods of detecting macrophages in the infarcted tissue can be very useful in the evaluation of MI both clinically and in the assessment of new therapies.

Imaging plays a central role in assessing the structure and function of heart.[1,3] Due to its security and high spatial resolution, magnetic resonance imaging (MRI) can be the imaging modality of choice.[4] Traditionally, gadolinium contrast agents such as Gd-DTPA (diethylene triamine penlaacetic acid) have been commonly used in T_1-weighted MRI.[5a,b] However, these contrast agents have short half-life, low relaxivity and may lead to renal fibrosis.[5c] Furthermore, gadolinium as small molecule contrast agent is extracellular contrast agent, which fails in MRI of specific tissue such as MI.[5d] In contrary, magnetic iron oxide nanoparticles (Fe_3O_4) are biocompatible and biodegradable, which also show high saturation field, extra magnetic anisotropy contributions, and so on.[6] More importantly, many reports have indicated that iron oxide nanoparticles are able to be phagocytized by inflammatory cells.[7] For example, Sosnovik et al. have used iron oxide nanoparticles to label macrophages and detected MI by MRI.[8] Yet these iron oxide nanoparticles are polydisperse with poor magnetic properties and nontarget, which cannot realize highly sensitive MRI of MI. Recently, thermal decomposition process has become the commonly used synthesis method, as this process can provide uniformly and highly crystalline iron oxide nanocrystals such as iron oxide nanocubes, which are nanometer-sized and show high magnetic properties.[9] If iron oxide nanocubes can be designed as contrast agents, highly sensitive MRI of macrophages in the infarcted tissue would be achieved.

However, there are still challenges for nanocubes as contrast agents for MRI of MI. First, the nanocubes obtained by thermal decomposition are hydrophobic. It is of prime importance to stabilize the nanocubes by surface modification. Previously, we have synthesized 1,2-dioleoyl-sn-glycero-3-phosphoethanolaminen-[poly(ethylene glycol)] (DSPE-PEG) coated hydrophobic iron oxide nanoparticles which can be stable in water.[10] In a similar way, DSPE-PEG is able to stabilize nanocubes and PEG coating is incorporated to provide a good colloidal stability for nanocubes. Second, specific delivery of nanocubes to macrophages in the infarcted tissue is another challenge. In general, targeting molecules such as antibodies, peptides, and molecules are used to improve the ability of specific delivery. However, these targeting molecules on the surface of nanoparticles may change some properties such as size, potential, and so on. Magnetic targeting may facilitate accumulation of iron oxide nanocubes in heart, as iron oxide nanocubes have excellent magnetic properties. Therefore, taking these into consideration, water-stable iron oxide nanocubes can be designed as nanoplatforms with the ability of magnetic targeting to the heart and MRI of MI. Herein, we report magnetic field responsive nanocubes (MFRNs) in the application of an external magnetic field gradient to the infarcted tissue in order to therein accumulate magnetically responsive

B. Hu, J. Chen, Prof. X. Zhang
National Key Laboratory of Biochemical Engineering
Institute of Process Engineering
Chinese Academy of Sciences
Beijing 100190, P. R. China
E-mail: xzhang@ipe.ac.cn
M. Zeng, Prof. Z. Fan
Department of Radiology
Beijing An Zhen Hospital
Capital Medical University
Beijing Institute of Heart, Lung and Blood Vessel Disease
Beijing 100029, P. R. China
E-mail: fanzm120@126.com
J. Chen, Prof. Z. Zhang
School of Pharmaceutical Sciences
Zhengzhou University
Zhengzhou 450001, P. R. China
Prof. X. Zhang
Collaborative Innovation Center for Biotherapy
School of Medicine
Tsinghua University
Beijing 100084, P. R. China

DOI: 10.1002/smll.201600263

www.MaterialsViews.com

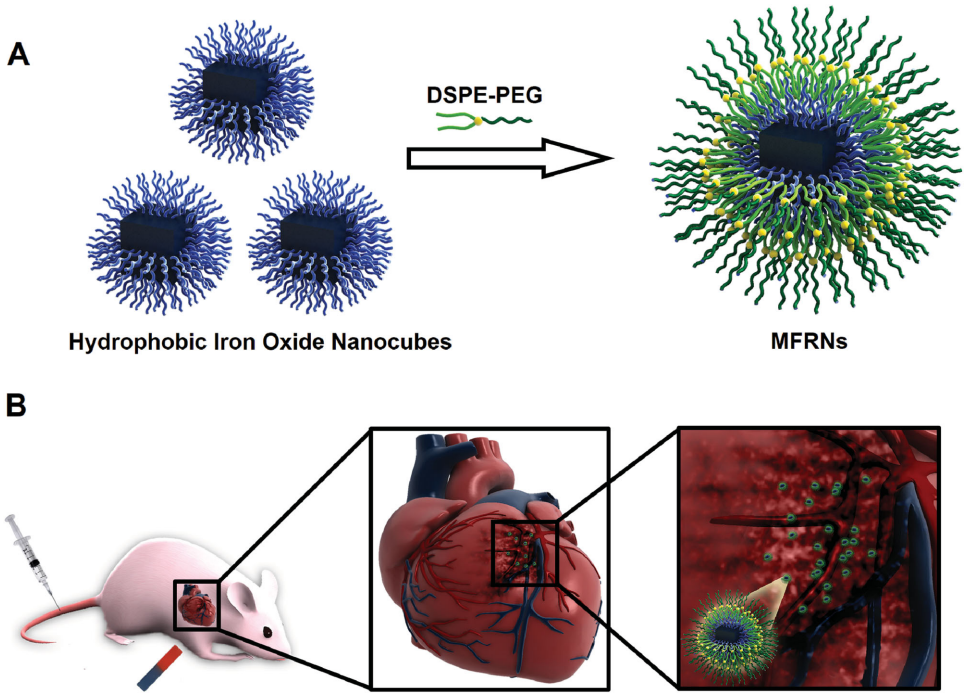

Scheme 1. A) The preparation of MFRNs: DSPE-PEG was used to improve the colloidal stability and biocompatibility of hydrophobic nanocubes through a micelle formation procedure. B) Schematic interpretation of MFRNs in vivo: intravenous injection of MFRNs accumulated in heart and infiltrated into the infarcted tissue under the influence of external magnetic field.

nanoscale systems. In this system, hydrophobic iron oxide nanocubes were stabilized by DSPE-PEG to improve colloidal stability and biocompatibility (**Scheme 1**A). As shown in Scheme 1B, after intravenous injection of MFRNs, a magnet was used to enhance the enrichment of iron oxide nanocubes in heart and phagocytosis of cardiac macrophages in the infracted tissue, which would facilitate MRI of MI.

The iron oxide nanocubes were first synthesized by high temperature thermal decomposition. The peaks of XRD (X-ray diffraction) corresponded to the standard powder diffraction files of magnetite (PDF#19-0629) and the crystalinity was about 98.27% (Figure S1, Supporting Information). The FT-IR (Fourier transform infrared spectroscopy) bonds of iron oxide nanocubes found at the following wavenumbers: 1028, 1404, 1638, 2850, 2919, and 3422 cm^{-1} which were from oleic acid and 4-biphenylcarboxylic acid (**Figure 1**A). The peak centered at 3422 cm^{-1} was from the —O—H group. The peaks at 2919, 2850, and 1404 cm^{-1} were corresponding to the $—CH_2$ and $—CH_3$ groups. The peak centered at 1638 cm^{-1} was from the —C=O group. The peak centered at 1028 cm^{-1} was assigned to the —C—O— group. As the nanocubes were hydrophobic, DSPE-PEG was used to improve their biocompatibility through a micelle formation procedure (Scheme 1A). FT-IR bonds of MFRNs found at the wavenumbers of 1111, 1348, 1463, 2853, 2918, and 3433 cm^{-1} which were from oleic acid, 4-biphenylcarboxylic acid, and DSPE-PEG (Figure 1B). The broad and strong stretching vibration band centered at 3433 cm^{-1} was corresponding to the —O—H group. The peaks centered at 2918 and 2853 cm^{-1} were assigned to the symmetric stretching of the $—CH_2$ and $—CH_3$ groups. The peak at 1463 and 1348 cm^{-1} were also due to the $—CH_2$ and $—CH_3$ groups. The characteristic peak centered at 1111 cm^{-1} originated from the —C—O—C— groups in PEG. The results of FT-IR showed that DSPE-PEG

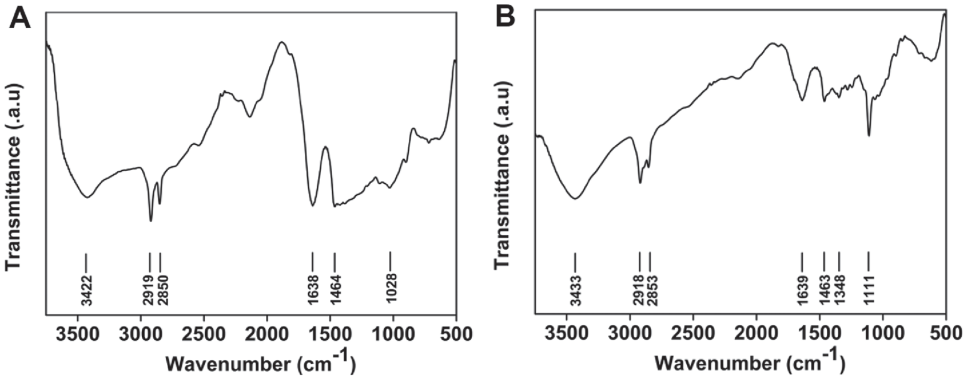

Figure 1. FT-IR spectra of A) iron oxide nanocubes and B) MFRNs. The transmittance was measured for the wavenumber from 500 to 3500 cm^{-1}.

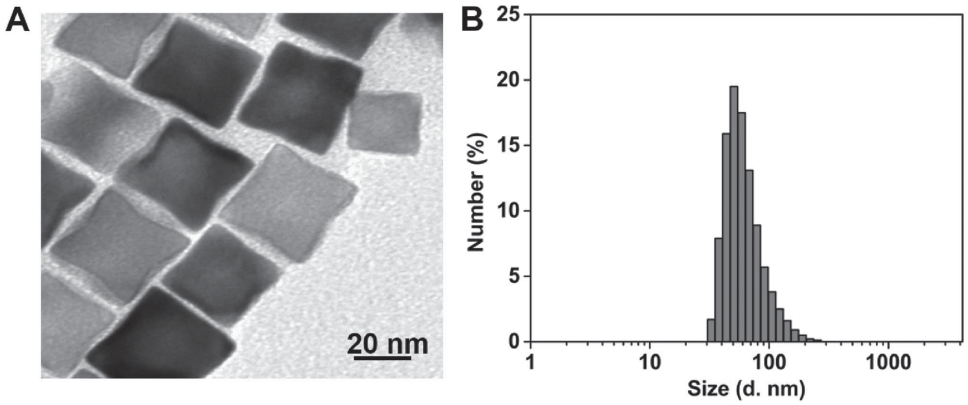

Figure 2. Characterization of MFRNs. A) The TEM image of MFRNs, and the scale bar corresponds to 20 nm. B) The hydrodynamic sizes and distribution of MFRNs measured by DLS in PBS (0.01 M, pH 7.4).

was successfully coated onto the surface of these nanoparticles. Furthermore, the results of thermal analysis curves also indicated the appearance of DSPE-PEG. As shown in Figure S3 (Supporting Information), only a slight weight loss occurred from 20 to 120 °C owing to the evaporation of physically adsorbed water and the weight loss from 120 to 300 °C was due to the decomposition of chemically bound water. The weight loss from 300 to 600 °C was the result of the breakdown of organic molecules such as oleic acid, 4-biphenylcarboxylic acid, and DSPE-PEG. Compared with iron oxide nanocubes, there was a percentage weight loss of 70% for MFRNs, which could attribute to the DSPE-PEG. The attachment of PEG onto the surface of magnetic nanoparticles had been shown to inhibit its uptake by the reticuloendothelial system and prolong circulation.[11] Furthermore, PEG would improve the contrast efficiency by enhancing water diffusion in close proximity to the nanoparticle core, provide appropriate biocompatibility, improve colloidal stability, and retain high r_2 values for MRI.[12]

The size of the MFRNs was confirmed by TEM (transmission electron microscope) and dynamic light scattering (DLS) analysis (**Figure 2**). The large magnification TEM image showed that MFRNs presented similar monodispersed and cubic-like structure with the diameters of about 40 nm (Figure 2A and Figure S2, Supporting Information). In agreement with the TEM results, the hydrodynamic sizes were about 65 nm and the PDI (polydispersity index) value was 0.395, which showed that the modification of DSPE-PEG coated iron oxide nanocubes did not change their dispersity (Figure 2B). In addition, the zeta potentials of nanoparticles were about −3.5 mV and close to electric neutrality. The serum stability was very important for the design of the MRI contrast agent. The MFRNs were incubated in PBS (phosphate buffered saline) containing 10% FBS (fetal bovine serum) and the hydrodynamic sizes were measured by DLS at different times (Figure S2A, Supporting Information). The size distribution of MFRNs changed slightly after incubation of 72 h (Figure S4B, Supporting Information). These results showed that MFRNs were stable without aggregation in serum, which indicated that the nanoparticles would have biocompatibility and stability in vivo.

To further assess magnetic properties for MRI application, the magnetization curve and r_2 value were measured. As shown in **Figure 3**A, magnetization curve exhibited no remnant magnetization and coercivity at room temperature and the saturation magnetization was about 60 emu g^{-1}. The inset picture showed that MFRNs accumulated on the cup wall under attraction of a magnet, which suggested that MFRNs were sensitive to magnetic field. In addition, as shown in Figure S5 (Supporting Information), the dispersity

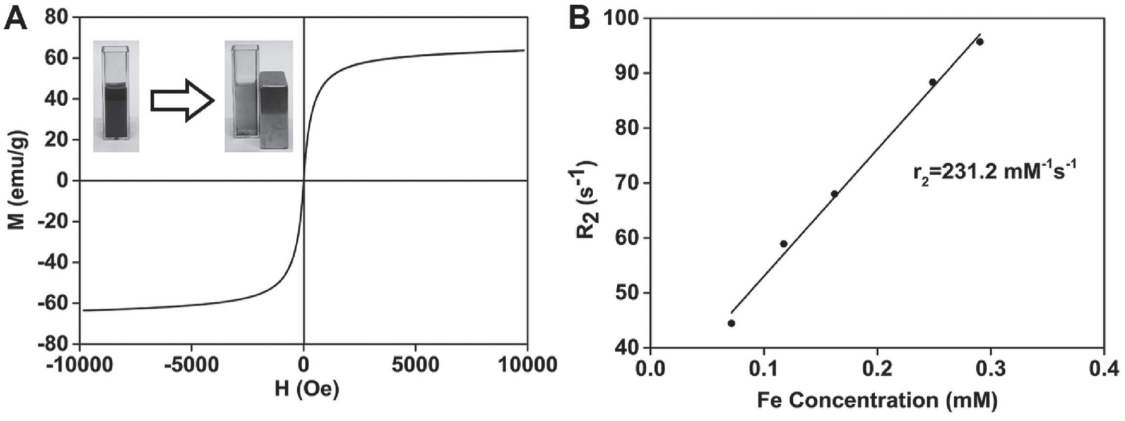

Figure 3. The magnetic properties of MFRNs. A) The magnetization curve of MFRNs. Inset picture showed the accumulation of MFRNs with the magnet. B) A plot of r_2 as a function of the Fe concentration of MFRNs. The slope of Fe concentration-R_2 regression curve was r_2 relaxivity.

www.MaterialsViews.com

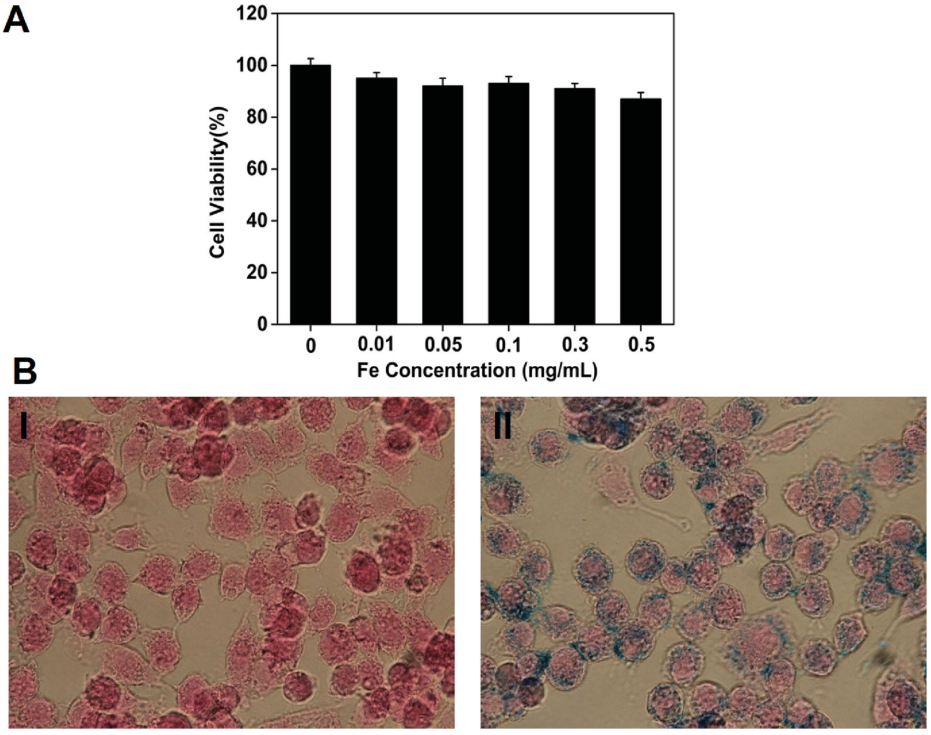

Figure 4. In vitro cell study. A) The cytotoxicity test of MFRNs. B) The Prussian blue staining of the RAW 264.7 cells incubated without (I) or with (II) MFRNs. The cells were red staining and MFRNs were blue staining in the cytoplasm.

of redispersed MFRNs after magnetic accumulation basically remains unchanged. Furthermore, the r_2 value was calculated by measuring the change of the spin–spin relaxation rate ($R_2 = 1/T_2$) per unit Fe concentration with a 1.5-T magnetic resonance analyzer. As shown in Figure 3B, the r_2 value of MFRNs was 231.2×10^{-3} M^{-1} s^{-1} which was higher than commercial contrast agents such as Resovist, which might lie in the fact that Resovist was obtained by the coprecipitation method while nanocubes were prepared under high temperature conditions.[13] The results of magnetic properties indicated that MFRNs were magnetic sensitive, which motivated us to examine the application of the magnetic nanocubes as a powerful contrast agent for in vivo MRI of MI.

Before in vivo imaging, the cytotoxicity and cellular uptake of MFRNs were tested. The cytotoxicity of MFRNs was evaluated with a cell counting kit using a mouse monocyte macrophage RAW264.7 cell line. As shown in **Figure 4**A, no appreciable toxicity was observed up to 0.5 mg Fe mL^{-1}, which demonstrated the excellent biocompatibility of MFRNs. The cellular uptake of MFRNs was confirmed through the Prussian blue staining after the incubation of RAW264.7 cells with MFRNs after 24 h. The MFRNs were readily internalized by the cells without any treatment to enhance cellular uptake, and they were observed in the cytoplasm as blue staining (Figure 4B). The results of cell experiments suggested that MFRNs were biocompatible and could be engulfed by macrophages, which promoted us to examine the magnetic resonance (MR) contrast ability of MFRNs.

The MI model was successfully built by permanently occluding the left main coronary artery with an intramural suture.[2d,e] As MI could lead to cellular necrosis and apoptosis and inflammation, the hematoxylin–eosin staining of hearts were executed. As shown in Figure S6B (Supporting Information), there were lots of inflammatory cells like macrophages infiltrated in the infracted tissue and degeneration or necrosis in the myocardium, while there was no inflammation and injury observed in the heart of control rats (Figure S6A, Supporting Information). Based on the magnetic properties and endocytosis experiment, MFRNs were chosen for T_2* MRI of MI by a 7-T MRI scanner. 48 h after MI, rats were injected with MFRNs intravenously under anesthesia and a 0.4-T magnet (30 mm × 25 mm × 12 mm) was put on the heart for 4 h to enhance the enrichment of MFRNs and phagocytosis of cardiac macrophages in the infracted tissue (Figure S7, Supporting Information). As shown in **Figure 5**A, the presence of negative contrast enhancement (white arrows), consistent with the accumulation of the MFRNs could be seen clearly in the infarcted myocardium, which indicated the ability of MFRNs to target the infarct and be engulfed by cardiac macrophages. In comparison, with magnet-exposure, there was more negative contrast enhancement in the infarcted tissue, demonstrating the magnet improved the accumulation of MFRNs in the infarcted myocardium and the image of MRI consistently revealed the presence of left ventricular dilatation with thinning and akinesis of the anterior, lateral, and inferolateral walls of the left ventricle. In order to quantitatively assess the MR contrast due to MFRNs accumulation in the infarcted myocardium, the relative T_2* MRI signal intensity of MRI was determined before and after injection of MFRNs (Figure 5B). After injection, the signal intensity was diminished by 25% and 65%, respectively, without or with magnet-exposure. The results of MRI suggested that MFRNs were responsive to external magnetic field and provided a powerful tool for MRI of MI.

To better understand the accumulation of MFRNs in the infarcted myocardium under the influence of external magnetic field, the hearts were harvested and stained by the Prussian blue after MRI. As shown in **Figure 6**B, blue staining of MFRNs were observed in the infarcted myocardium with magnet-exposure whereas few nanocubes were observed in the infarcted myocardium without magnet-exposure (Figure 6A). In addition, Prussian blue staining of the liver and spleen with and without magnet-exposure was carried out. There were lots of MFRNs observed in liver and spleen without magnet-exposure because nanoparticles could accumulate in liver and spleen passively, whereas few MFRNs observed with magnet-exposure

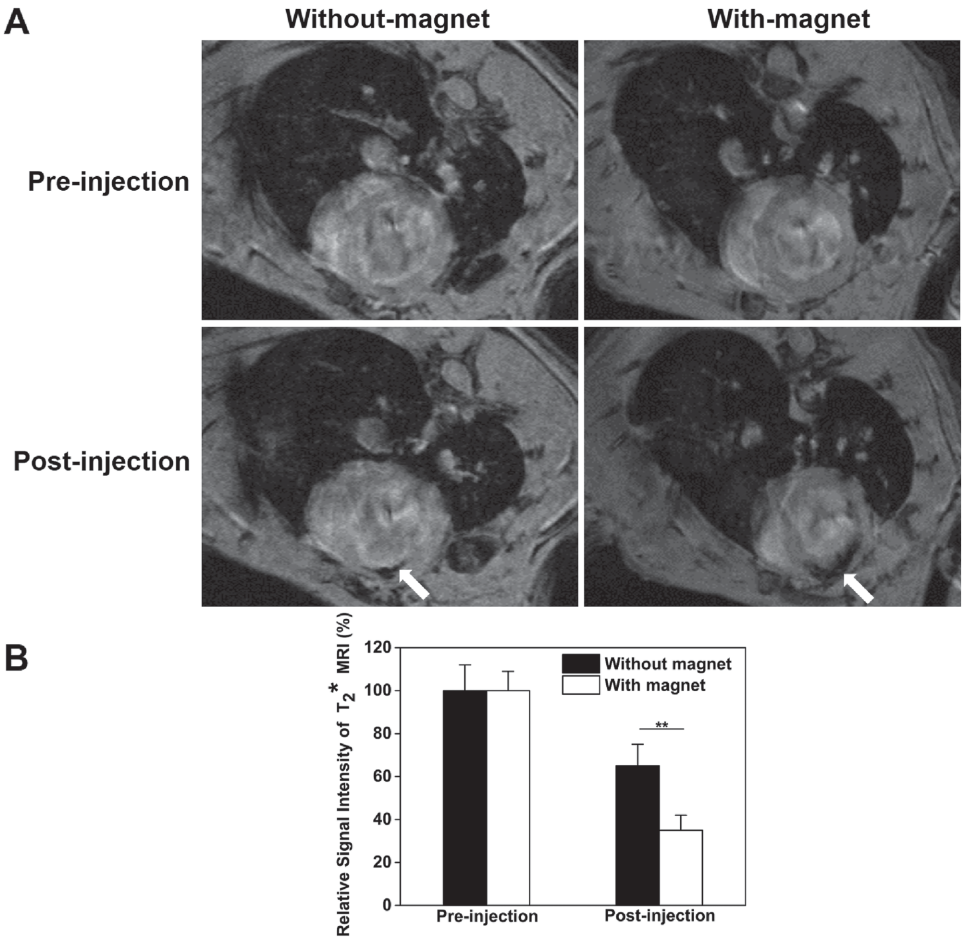

Figure 5. In vivo MRI of MI. A) Representative in vivo 7 Tesla MR images of hearts before and 24 h after intravenous injection of MFRNs without or with magnet-exposure. The white arrows pointed the infarcted tissue. B) Relative signal intensity of T_2* MRI in the infarcted tissue before and 24 h after intravenous injection of MFRNs without or with magnet-exposure. (**$p < 0.01$).

as MFRNs mostly accumulated in heart (Figure S8, Supporting Information). These results also indicated the improvement of accumulation of MFRNs in the infarcted myocardium under the influence of external magnetic field.

In summary, we successfully developed external magnetic field responsive MFRNs as nanoplatforms for MRI monitoring and external magnetic field-induced selective targeting of macrophages in the infarcted tissue. The MFRNs had uniform size, favorable colloidal stability and high magnetic properties. Both in vitro and in vivo experiments were performed to justify the biocompatibility and ability of magnetic target to heart of MFRNs. More importantly, under the influence of external magnetic field, MFRNs performed qualitative and quantitative MRI of MI. As nanoprobes, MFRNs would have clinical practicality, which provided more efficient and safe diagnostics systems of MI and if study could be more in-depth and the costs could be further reduced, there would be more popular

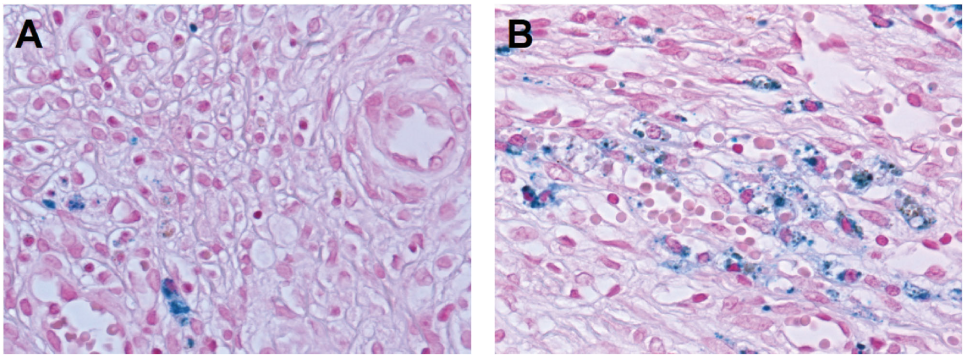

Figure 6. The histological Prussian blue staining of the infarcted myocardium after MRI A) without or B) with magnet-exposure. The cells in tissue were red staining and MFRNs were blue staining intracell.

applications. In addition, as the responsiveness to magnetic field, iron oxide nanocubes would provide potential delivery systems of probes and drugs for applications of diagnosis and treatment.

Supporting Information

Supporting Information is available from the Wiley Online Library or from the author.

Acknowledgements

B.H. and M.Z. contributed equally to this work. This work was financially supported by the National Natural Science Foundation of China (21304099, 51203162, 51373177), the National High Technology Research and Development Program (2014AA020708, 2012AA022703, 2012AA020804), the Instrument Developing Project of the Chinese Academy of Sciences (YZ201253, YZ201313), the Open Funding Project of the National Key Laboratory of Biochemical Engineering (Y22504A169), the "Strategic Priority Research Program" of the Chinese Academy of Sciences (XDA09030301-3), and Beijing Natural Science Foundation (Grant no. Z141100000214010). All procedures involving experimental animals were performed in accordance with protocols approved by the Institutional Animals Care and Use Committee of Peking University.

[1] G. A. Gray, C. I. White, A. Thomson, A. Kozak, C. Moran, M. A. Jansen, *Exp. Physiol.* **2013**, *98*, 606.

[2] a) R. C. Scott, J. M. Rosano, Z. Ivanov, B. Wang, P. L. Chong, A. C. Issekutz, D. L. Crabbe, M. F. Kiani, *FASEB J.* **2009**, *23*, 3361; b) J. M. Rosano, R. Cheheltani, B. Wang, H. Vora, M. F. Kiani, D. L. Crabbe, *Cardiovasc. Eng. Technol.* **2012**, *3*, 237; c) N. K. Naresh, T. Ben-Mordechai, J. Leor, F. H. Epstein, *Curr. Cardiovasc. Imaging Rep.* **2011**, *4*, 63; d) N. K. Naresh, Y. Q. Xu, A. L. Klibanov, M. H. Vandsburger, C. H. Meyer, J. Leor, C. M. Kramer, B. A. French, F. H. Epstein, *Radiology* **2012**, *264*, 428; e) T. Harel-Adar, T. Ben Mordechai, Y. Amsalem, M. S. Feinberg, J. Leor, S. Cohen, *Proc. Natl. Acad. Sci. USA* **2011**, *108*, 1827.

[3] A. Barison, C. Grigoratos, G. Todiere, G. D. Aquaro, *Heart Fail. Rev.* **2015**, *20*, 731.

[4] a) E. Terreno, D. Delli Castelli, A. Viale, S. Aime, *Chem. Rev.* **2010**, *110*, 3019; b) D. E. Sosnovik, M. Nahrendorf, R. Weissleder, *Circulation* **2007**, *115*, 2076.

[5] a) J. Xu, S. L. Gai, P. A. Ma, Y. L. Dai, G. X. Yang, F. He, P. P. Yang, *J. Mater. Chem. B* **2014**, *2*, 1791; b) P. Sharma, N. E. Bengtsson, G. A. Walter, H. B. Sohn, G. Y. Zhou, N. Iwakuma, H. D. Zeng, S. R. Grobmyer, E. W. Scott, B. M. Moudgil, *Small* **2012**, *8*, 2856; c) M. Mahmoudi, H. Hosseinkhani, M. Hosseinkhani, S. Boutry, A. Simchi, W. S. Journeay, K. Subramani, S. Laurent, *Chem. Rev.* **2011**, *111*, 253; d) G. Ferrauto, E. Di Gregorio, W. Dastru, S. Lanzardo, S. Aime, *Biomaterials* **2015**, *58*, 82.

[6] a) F. Schulze, A. Dienelt, S. Geissler, P. Zaslansky, J. Schoon, K. Henzler, P. Guttmann, A. Gramoun, L. A. Crowe, L. Maurizi, J. P. Vallee, H. Hofmann, G. N. Duda, A. Ode, *Small* **2014**, *10*, 4340; b) N. Lee, T. Hyeon, *Chem. Soc. Rev.* **2012**, *41*, 2575; c) L. H. Reddy, J. L. Arias, J. Nicolas, P. Couvreur, *Chem. Rev.* **2012**, *112*, 5818.

[7] a) Y. Q. Zhong, F. Y. Dai, H. Deng, M. H. Du, X. N. Zhang, Q. J. Liu, X. Zhang, *J. Mater. Chem. B* **2014**, *2*, 2938; b) F. Y. Dai, M. H. Du, Y. G. Liu, G. Y. Liu, Q. J. Liu, X. Zhang, *J. Mater. Chem. B* **2014**, *2*, 2240.

[8] D. E. Sosnovik, M. Nahrendorf, N. Deliolanis, M. Novikov, E. Aikawa, L. Josephson, A. Rosenzweig, R. Weissleder, V. Ntziachristos, *Circulation* **2007**, *115*, 1384.

[9] a) J. Park, K. An, Y. Hwang, J. G. Park, H. J. Noh, J. Y. Kim, J. H. Park, N. M. Hwang, T. Hyeon, *Nat. Mater.* **2004**, *3*, 891; b) M. V. Kovalenko, M. I. Bodnarchuk, R. T. Lechner, G. Hesser, F. Schaffler, W. Heiss, *J. Am. Chem. Soc.* **2007**, *129*, 6352; c) D. Kim, N. Lee, M. Park, B. H. Kim, K. An, T. Hyeon, *J. Am. Chem. Soc.* **2009**, *131*, 454.

[10] a) B. B. Hu, F. Y. Dai, Z. M. Fan, G. H. Ma, Q. W. Tang, X. Zhang, *Adv. Mater.* **2015**, *27*, 5499; b) Y. D. Jin, C. X. Jia, S. W. Huang, M. O'Donnell, X. H. Gao, *Nat. Commun.* **2010**, *1*, 41.

[11] a) H. Y. Wen, C. Y. Dong, H. Q. Dong, A. J. Shen, W. J. Xia, X. J. Cai, Y. Y. Song, X. Q. Li, Y. Y. Li, D. L. Shi, *Small* **2012**, *8*, 760; b) M. P. Leal, S. Rivera-Fernandez, J. M. Franco, D. Pozo, J. M. de la Fuente, M. L. Garcia-Martin, *Nanoscale* **2015**, *7*, 2050.

[12] a) J. F. Zeng, L. H. Jing, Y. Hou, M. X. Jiao, R. R. Qiao, Q. J. Jia, C. Y. Liu, F. Fang, H. Lei, M. Y. Gao, *Adv. Mater.* **2014**, *26*, 2694; b) Y. C. Park, J. B. Smith, T. Pham, R. D. Whitaker, C. A. Sucato, J. A. Hamilton, E. Bartolak-Suki, J. Y. Wong, *Colloids Surf., B* **2014**, *119*, 106.

[13] R. R. Qiao, C. H. Yang, M. Y. Gao, *J. Mater. Chem.* **2009**, *19*, 6274.

Received: January 27, 2016
Revised: April 1, 2016
Published online: May 4, 2016